doi:10.1093/brain/awx375 BRAIN 2018: 141; 673–687 | 673

BRAIN
A JOURNAL OF NEUROLOGY

HDAC6 is a therapeutic target in mutant GARS-induced Charcot-Marie-Tooth disease

Veronick Benoy,[1,2] Lawrence Van Helleputte,[1,2] Robert Prior,[1,2] Constantin d'Ydewalle,[1,2] Wanda Haeck,[1,2] Natasja Geens,[1,2] Wendy Scheveneels,[1,2] Begga Schevenels,[1,2] M. Zameel Cader,[3,4] Kevin Talbot,[3] Alan P. Kozikowski,[5] Pieter Vanden Berghe,[6] Philip Van Damme,[1,2,7] Wim Robberecht[1,2,7] and Ludo Van Den Bosch[1,2]

Peripheral nerve axons require a well-organized axonal microtubule network for efficient transport to ensure the constant crosstalk between soma and synapse. Mutations in more than 80 different genes cause Charcot-Marie-Tooth disease, which is the most common inherited disorder affecting peripheral nerves. This genetic heterogeneity has hampered the development of therapeutics for Charcot-Marie-Tooth disease. The aim of this study was to explore whether histone deacetylase 6 (HDAC6) can serve as a therapeutic target focusing on the mutant glycyl-tRNA synthetase (GlyRS/*GARS*)-induced peripheral neuropathy. Peripheral nerves and dorsal root ganglia from the C201R mutant *Gars* mouse model showed reduced acetylated α-tubulin levels. In primary dorsal root ganglion neurons, mutant GlyRS affected neurite length and disrupted normal mitochondrial transport. We demonstrated that GlyRS co-immunoprecipitated with HDAC6 and that this interaction was blocked by tubastatin A, a selective inhibitor of the deacetylating function of HDAC6. Moreover, HDAC6 inhibition restored mitochondrial axonal transport in mutant GlyRS-expressing neurons. Systemic delivery of a specific HDAC6 inhibitor increased α-tubulin acetylation in peripheral nerves and partially restored nerve conduction and motor behaviour in mutant *Gars* mice. Our study demonstrates that α-tubulin deacetylation and disrupted axonal transport may represent a common pathogenic mechanism underlying Charcot-Marie-Tooth disease and it broadens the therapeutic potential of selective HDAC6 inhibition to other genetic forms of axonal Charcot-Marie-Tooth disease.

1 KU Leuven - University of Leuven, Department of Neurosciences, Experimental Neurology, and Leuven Research Institute for Neuroscience & Disease (LIND), Leuven, Belgium
2 VIB - Center for Brain and Disease Research, Laboratory of Neurobiology, Leuven, Belgium
3 Nuffield Department of Clinical Neurosciences, University of Oxford, John Radcliffe Hospital, Oxford, UK
4 The Weatherall Institute of Molecular Medicine, University of Oxford, John Radcliffe Hospital, Oxford, UK
5 Department of Medicinal Chemistry and Pharmacognosy, Drug Discovery Program, University of Illinois at Chicago, Chicago, USA
6 Translational Research Center for Gastrointestinal Disorders, University of Leuven, Leuven, Belgium
7 University Hospitals Leuven, Department of Neurology, Leuven, Belgium

Correspondence to: Ludo Van Den Bosch
Laboratory of Neurobiology
Campus Gasthuisberg O&N4, PB602
Herestraat 49
B-3000 Leuven
Belgium
E-mail: ludo.vandenbosch@kuleuven.vib.be

Received June 13, 2017. Revised October 26, 2017. Accepted November 20, 2017. Advance Access publication February 5, 2018

Keywords: Charcot-Marie-Tooth disease; GARS; HDAC6; acetylated α-tubulin; axonal transport

Abbreviations: CMAP = compound muscle action potential; CMT = Charcot-Marie-Tooth disease; DRG = dorsal root ganglion; GlyRS = glycyl-tRNA synthetase; SNAP = sensory nerve action potential

Introduction

Charcot-Marie-Tooth disease (CMT) is the most common inherited disorder of the peripheral nervous system, affecting ~1 in 2500 persons (Skre, 1974). Progressive motor axon degeneration leads to muscle weakness and wasting, muscle cramps and steppage gait. Typical deformities are *pes cavus*, hammertoes and clawed hands. Sensory nerve axon degeneration causes loss of sensation on the level of temperature, touch, vibration and pain (Skre, 1974). There is a wide genetic and clinical heterogeneity among patients (Reilly, 2007). At the genetic level, mutations in more than 80 genes can cause CMT. At the clinical level, patients are classified as CMT type 1 'CMT1', primarily caused by demyelination of peripheral nerve axons, or as CMT type 2 'CMT2', characterized by predominant axonal loss. Moreover, patients can have clinical features of both CMT1 and CMT2 and are then classified as 'intermediate CMT'. When only motor axons are affected, the disorder is referred to as distal hereditary motor neuropathy (distal HMN). Currently, no curative treatment for these patients exists.

Defects in axonal transport are often associated with neurodegeneration and with peripheral neuropathies in particular (Pareyson *et al.*, 2015; Prior *et al.*, 2017). Microtubules are used as molecular tracks to guide delivery of cargoes such as newly synthesized proteins, lipids, RNA and organelles to different parts of the cell (De Vos *et al.*, 2008). These structures are also required for the clearance of damaged organelles by cellular degradation mechanisms (Gibbs *et al.*, 2015). This cellular transport is crucial in neurons as it ensures the crosstalk between the soma and the synapse through the axon and as transport of mitochondria is essential to meet the high energy demands at the synapse. The acetylation of α-tubulin within the microtubules promotes the anchoring of the molecular motor kinesin and stimulates vesicular transport along the microtubules (Gibbs *et al.*, 2015). Histone deacetylase 6 (HDAC6) belongs to the class IIb HDACs and controls the acetylation status of several proteins such as α-tubulin. Targeting the activity or expression of HDAC6 has been shown to be beneficial in several neurodegenerative disorders such as Alzheimer's disease and amyotrophic lateral sclerosis (ALS), but also in CMT (d'Ydewalle *et al.*, 2011; Govindarajan *et al.*, 2013; Taes *et al.*, 2013; Zhang *et al.*, 2014; Guo *et al.*, 2017).

Previously, we demonstrated mitochondrial transport defects in dorsal root ganglion (DRG) neurons and reduced acetylation of α-tubulin in a mouse model for CMT2F, caused by mutations in small heat shock protein B1 (*HSPB1*) (d'Ydewalle *et al.*, 2011). These mice overexpress mutant human HSPB1 specifically in neurons and develop motor and sensory symptoms reminiscent to what is seen in patients. Selective inhibition of the deacetylating function of HDAC6 normalized the acetylation of α-tubulin, as well as the axonal transport defects. Moreover, HDAC6 inhibition also restored the motor and sensory defects in symptomatic $HSPB1^{S135F}$ mice (d'Ydewalle *et al.*, 2011).

CMT or related peripheral neuropathies can also be caused by mutations in aminoacyl transfer RNA (tRNA) synthetases (aaRS). These ubiquitously expressed enzymes ensure the coupling of tRNA molecules to their cognate amino acids, which is crucial for correct protein translation (Guo *et al.*, 2010). Mutations in *GARS* have not only been identified in patients classified as autosomal-dominant CMT2D, but can also cause distal HMN (Antonellis *et al.*, 2003). Although glycyl-tRNA synthetase (GlyRS, encoded by *GARS*) is an essential and ubiquitously expressed 'house-keeping' enzyme (Yao and Fox, 2013), an endogenous mutation in *Gars* causes specific degeneration of motor and sensory nerves in mice (Seburn *et al.*, 2006; Achilli *et al.*, 2009). Moreover, mutations in other members of the aaRS family can lead to the development of related neuropathies in humans (Jordanova *et al.*, 2006; Latour *et al.*, 2010; McLaughlin *et al.*, 2010; Gonzalez *et al.*, 2013; Vester *et al.*, 2013). This strongly indicates that peripheral nerve axons are specifically vulnerable for mutations in aaRS. Using *Drosophila* models to study mutant GlyRS and mutant TyrRS-induced toxicity, common genetic modifiers were discovered, indicative for a shared mechanism responsible for the tRNA synthetase-induced peripheral neuropathies (Ermanoska *et al.*, 2014). Several studies addressed the question whether CMT2-causing mutations affect the canonical aminoacylation activity of GlyRS, inducing axonal degeneration. Yeast complementation and radioactive assays showed that only a selection of mutations found in patients alter this activity (Jordanova *et al.*, 2006; Stum *et al.*, 2011; Griffin *et al.*, 2014). Heterozygous mice expressing C201R mutant GlyRS did not show decreased aminoacylation activity of GlyRS (Achilli *et al.*, 2009). Moreover, overexpression of wild-type GlyRS in two mutant GlyRS-induced mouse models for CMT did not rescue the motor and sensory phenotype (Motley *et al.*, 2011). Defects in protein translation, observed in a CMT *Drosophila* model expressing mutant GlyRS could not be correlated to altered aminoacylation activity of the different GlyRS mutants, nor could be rescued by overexpression of wild-type GlyRS (Niehues *et al.*, 2015). Altogether, the pathogenic mechanism underlying aaRS-induced axonal toxicity does not seem to be solely related to aminoacylation.

The aim of this study was to investigate the therapeutic potential of selective HDAC6 inhibition in other forms of CMT. In addition, we wanted to explore whether different genetic forms of CMT share common pathological hallmarks, indicative of a general underlying pathogenic mechanism. We focused on mutant *GARS*-induced CMT2D and discovered that GlyRS and HDAC6 co-immunoprecipitate, an interaction that was blocked by tubastatin A. Moreover, reduction of GlyRS reduced HDAC6 protein levels and vice versa. We used a previously established mouse model (Achilli *et al.*, 2009) to investigate the effects of HDAC6 inhibition in mutant *GARS*-induced CMT2. These mice carry an endogenous mutation in *Gars* and develop motor and sensory axonal degeneration from early age on. On the pathological level, we found decreased acetylation of α-tubulin in peripheral nervous tissue. Cultured DRG neurons showed aberrant mitochondrial transport and tubastatin A improved the acetylation of α-tubulin, as well as the axonal transport of mitochondria. Moreover, this selective HDAC6 inhibitor also improved motor and sensory behaviour and enhanced reinnervation in the mutant *Gars* mice. Altogether, our data broaden the therapeutic potential of HDAC6 inhibition and point towards axonal transport defects as a common pathological mechanism in CMT.

Materials and methods

Cell culture

Mouse neuroblastoma cells (N2a, ATCC, CCL-131) were grown in a 1:1 mixture of DMEM (Dulbecco's modified Eagle medium) and F12 medium supplemented with GlutaMAX™ (Thermo Fisher Scientific), 100 µg/ml streptomycin, 100 U/ml penicillin (Thermo Fisher Scientific), 10% foetal calf serum (Greiner Bio-One), 1% non-essential amino acids (Thermo Fisher Scientific), and 1.6% $NaHCO_3$ (Thermo Fisher Scientific) at 37°C and 7.5% CO_2. To split the cells, cells were washed with Versene (Thermo Fisher Scientific) and dissociated with 0.05% Trypsine-EDTA (Thermo Fisher Scientific).

Primary DRG neurons were cultured from 12-month-old mice. The DRG neurons were dissected from the spinal cord and kept in cold Hibernate® A (Thermo Fisher Scientific) supplemented with B27 (Thermo Fisher Scientific), hereafter referred to as HA/B27. To extract the DRG neurons, the tissue was dissociated by a 45 min incubation in the presence of 2 mg/ml papain (LS003119, Worthington Biochemical Corp.) and thorough resuspension until all tissue was dissolved. The cell suspension was added to a gradient solution containing four layers of 37%, 25%, 20% and 15% OptiPrep™ Density Gradient Medium (Sigma-Aldrich) in HA/B27 and centrifuged during 15 min at 800*g* without the brake. The cell suspension was subsequently washed in HA/B27. An additional centrifugation step was performed during 4 min at 400*g* and the cells were plated in culture medium containing Neurobasal® A (Thermo Fisher Scientific) supplemented with B27 (Thermo Fisher Scientific), 200 mM L-glutamine (Thermo Fisher Scientific), 68 ng/ml neurite growth factor (Merck Millipore) and antibiotics. The N2a cells and DRG neurons were treated overnight at 37°C with tubastatin A (provided by A. Kozikowski, University of Illinois, Chicago) (Butler *et al.*, 2010) or an equivalent amount of DMSO (Sigma-Aldrich).

Primary motor neurons were obtained by dissecting the spinal cords from Embyonic Day 13.5 mouse embryos in Hanks' Balanced Salt Solution (HBSS, Thermo Fisher Scientific) followed by removal of the meninges and the dorsal root ganglia. After digestion of ventral cord fragments (15 min; 0.05% Trypsin-EDTA, Thermo Fisher Scientific at 37°C) and treatment with DNase (Sigma-Aldrich), the tissue was further dissociated by trituration. The cell suspension was layered on 6.2% OptiPrep™ (Sigma-Aldrich) and centrifuged at 500*g* for 15 min. The band on top of the OptiPrep™ cushion was resuspended and centrifuged for 20 min at 75*g* on a 4% BSA cushion. The cells from the pellet were plated in Neurobasal® A (Thermo Fisher Scientific) supplemented with B27, horse serum (2%), L-glutamine, CNTF (0.4 ng/ml; Peprotech), GDNF (0.4 ng/ml, Peprotech), BDNF (0.4 ng/ml, Peprotech) and antibiotics.

RNA interference-mediated knock down

Cells were plated at a density of 500 000 cells per condition, 24 h prior to transfection. Transfection of N2a cells was performed using Lipofectamine™ 2000 (Thermo Fisher Scientific), in serum- and antibiotic-free condition using OptiMem™ I Reduced Serum medium (Thermo Fisher Scientific), according to manufacturer's instructions. Small interfering RNA technology, comprising three different siRNA molecules and one control siRNA molecule, was used to target GlyRS expression (SR419603, Origene). Bioinformatic tools (Ryan *et al.*, 2008; and BLAST – US National Library of Medicine) were used to check specificity of the siRNAs towards mouse *Gars* mRNA. Plasmids containing short hairpin (sh)RNA molecules directed against mouse *Hdac6* mRNA or a scrambled short hairpin (sh)RNA (Origene) were used. At different time points (24 h, 48 h and 72 h post-transfection) the cells were collected for quantitative PCR or western blot analysis.

Reverse transcription quantitative PCR

Total RNA was extracted from N2a cells on different time points after transfection using RNeasy® Mini kit (Qiagen) according to the manufacturer's instructions. Reverse transcription was performed with the SuperScript® III Reverse Transcriptase assay (Thermo Fisher Scientific) according to the manufacturer's instructions, using 0.5 µg total RNA. For RT-qPCR analysis, three different reference genes and two target genes were selected for evaluation of their expression profile using exon-spanning TaqMan™ gene expression assays (Applied Biosystems): polymerase (RNA) II Subunit A (*Polr2a*), hypoxanthine-guanine phosphoribosyltransferase (*Hprt*), glyceraldehyde 3-phosphate dehydrogenase (*Gapdh*), glycyl-tRNA synthetase (*Gars*) and histone deacetylase 6 (*Hdac6*). A master mix for each PCR run was prepared containing TaqMan™ Fast Universal PCR Master Mix (2×, no AmpErase UNG, Applied Biosystems) and 1/20 diluted cDNA

was added. All samples were amplified in triplicate from the same cDNA preparation and the mean values were calculated. The stability of the expression of the housekeeping genes was evaluated by geometric averaging of multiple internal controls (geNorm) (Vandesompele *et al.*, 2002) and qBaseplus software (Biogazelle, Ghent, Belgium) and a combination of minimum two housekeeping genes was used to normalize the expression of the target genes.

Co-immunoprecipitation

For immunoprecipitation, cells were plated at a density of 6×10^6 cells per dish, 24 h prior to transfection. Cells were transfected using TransIT-Neural® Transfection Reagent (Mirus Bio), according to manufacturer's instructions in serum- and antibiotic-free conditions. The following plasmids were used: pCMV-DDK-tagged human cDNA encoding wild-type or C175R mutant GlyRS or pCMV-dsRED-tagged human cDNA encoding HDAC6.

Cells were collected 24 h post-transfection in RIPA buffer (radio-immunoprecipitation assay buffer containing 50 mM Tris, 150 mM NaCl, 0.5% Sodium deoxycholate, 0.1% SDS, 1% NP40) supplemented with protease inhibitors (cOmplete™, EDTA free, Roche). Anti-DDK M2 affinity Gel (Sigma-Aldrich) was used to immunoprecipitate DDK-tagged proteins and the protein complexes were analysed by western blot.

Western blot

Cells were washed with phosphate-buffered saline (PBS) and collected using RIPA buffer supplemented with a protease inhibitor cocktail (cOmplete™, EDTA-free Protease Inhibitor Cocktail, Sigma-Aldrich). Tissues were dissected from the mice and snap-frozen in liquid nitrogen. Dissociation of the tissue was achieved by using tubes containing LysisMatrix D beads (MagNA Lyser, Roche Diagnostics). Protein concentrations were determined using microBCA kit (Thermo Fisher Scientific) according to the manufacturer's instructions.

Before separating the samples on a 12% SDS-PAGE gel, reducing sample buffer (Thermo Fisher Scientific) was added to samples containing equal amounts of protein and these samples were boiled at 95°C for 5 min. After electrophoresis, the proteins were transferred to a polyvinylidene difluoride (PVDF) membrane (Merck Millipore). The non-specific binding was blocked by incubation of the membrane in 5% bovine serum albumin (BSA, SERVA Electrophoresis), diluted in Tris-buffered saline-Tween (TBS-T, 50 mM Tris, 150 mM NaCl, 0.1% Tween-20) for 1 h at room temperature followed by incubation with primary antibodies overnight.

The antibodies, diluted in TBS-T, were directed against α-tubulin (Sigma-Aldrich, T6199, 1/5000, 1 h), acetylated α-tubulin (Sigma-Aldrich, T6793, 1/5000, 1 h), calnexin (Enzo life Sciences, ADI-SPA-860-F, 1/1000, 1 h), gapdh (Ambion, Thermo Fisher Scientific, AM4300, 1/5000, 1 h), GlyRS (ProteinTech, 15831-1-AP, 1/500, overnight), HDAC6 (Cell Signaling, 7612S, 1/500, overnight) and DDK-tag (Sigma-Aldrich, F1804, 1/1000, 1 h). The secondary antibodies, coupled to horseradish peroxidase [anti-mouse or anti-rabbit, 1/5000, Agilent Technologies (Dako)], were used to detect the signal of the primary antibodies. Blots were visualized by adding the Enhanced Chemical Luminescence substrate (Thermo Fisher Scientific) and imaged on the ImageQuant™ LAS 4000 (GE Healthcare). A mild reblotting buffer (Merck Millipore) was applied to strip the blots. ImageQuant™ TL version 7.0 software was used to quantify the blots.

Immunocytochemistry

Cells were fixed by applying 4% paraformaldehyde (PFA) solution for 20 min and were permeabilized with 2 mg/ml BSA (Serva) diluted in 0.2 % Triton™ X-100/PBS during 10 min on ice. Non-specific binding was blocked by 3% BSA diluted in 0.02 % Triton™ X-100/PBS (blocking solution) during 30 min. Primary and secondary antibodies were diluted in blocking solution.

The following primary antibodies, dilutions and incubation times were used: anti-acetylated α-tubulin (Sigma-Aldrich, T6793, 1/5000, 1 h), GlyRS (ProteinTech, 15831-1-AP, 1/500, overnight) and anti-neuronal class III β-tubulin (BioLegend, 802001, 1/500, overnight). The following secondary antibodies, corresponding dilutions and incubation times were used: donkey anti-mouse IgG (Alexa Fluor®-conjugated, Life Technologies, 1/5000, 1 h) or donkey anti-rabbit IgG (Alexa Fluor®-conjugated, Life Technologies, 1/5000, 1 h).

After subsequent washing with 1.5% BSA in 0.02% Triton™ X-100/PBS, the cover slips were mounted with DAPI-containing Vectashield (Vectorlabs Inc.) to visualize the nuclei. Fluorescent micrographs were taken using a Zeiss Axio Imager M1 microscope (Carl Zeiss AG) equipped with an AxioCam MRm3 camera (Carl Zeiss AG). All images and subsequent analysis were performed in a blinded manner.

Cell viability

DRG neuron cultures were prepared from 1-year-old mice and equal cell densities were seeded in 96-well assay plates. On culture Day 1, cells were treated with either vehicle or 1 μM tubastatin A. Assays were performed on culture Day 2. Cell viability was measured using the ATPlite™ luminescence assay system according to the manufacturer's instructions. The MUH assay was performed as described previously (Martin *et al.*, 2016). Briefly, DRG neurons were washed with PBS and incubated with 0.01 mg/ml MUH (4-methylumbelliferyl heptanoate, Sigma-Aldrich) dissolved in PBS for 30 min at 37°C. Fluorescence was measured at excitation 355 nm and emission 460 nm with a cut-off value of 455 nm.

Mice

All animals were housed under standard conditions according to the guidelines of the University of Leuven (KU Leuven) and bred to heterozygous state. All animal experiments were approved by the local ethical committee of the KU Leuven (P033/2014 and P185/2012) and conducted in a blinded manner. Tubastatin A (50 mg/kg, A. Kozikowski, Chicago, IL, USA) was administered through daily intraperitoneal injections in home cages. During animal experiments, measurements to meet the requirements of replacement, refinement or reduction (the 3Rs) were implemented. In all behavioural experiments, equal numbers of male and female *Gars*$^{C201R/+}$ or littermate control mice (strain: C57Bl6/J) were used. Animal studies were performed blinded as the investigator was unaware of the genotypes of the mice. During tubastatin A treatments the different solution were blinded by a second

investigator. During drug treatments no adverse effects were observed and no animals were excluded from behavioural analysis.

For genotyping, genomic DNA was purified from mouse tails by lysing the tissue overnight at 55°C with 20 mg/ml proteinase K (Thermo Fisher Scientific) in a lysis buffer containing 100 mM Tris-HCl (pH 8.5), 5 mM EDTA, 0.2% SDS and 200 mM NaCl. After centrifugation, DNA was precipitated using isopropanol followed by centrifugation. Pellets were washed in 75% ethanol and dissolved in Tris-EDTA buffer containing 10 mM Tris-HCl (pH 7.5) and 0.1 mM EDTA. The *Gars*$^{C201R/+}$ mice were maintained in a C57Bl6/J genetic background (Achilli *et al.*, 2009). Genotyping of the *Gars*$^{C201R/+}$ mice was done by single nucleotide polymorphism genotyping using a FAM-labelled probe recognizing the C201R allele (5′-GCAGACGCATACCTTTCAACAG-3′) and a VIC-labelled probe recognizing the wild-type allele (5′-CT CGGAAGCACTCTC-3′).

Behavioural testing

General motor performance was assessed by placing the mice on an accelerating rotarod (Ugo Basile) with increasing speed from 4 rpm to 40 rpm in 5 min. The time spent on the rotarod was measured and for all mice the average of three consecutive trials without prior training was calculated.

Dynamometer (Chatillon Force Measurements, Ametek) in combination with either a grid (all paws) or a triangle (forepaws) was used to measure grip strength of the mice. For each mouse, the average of five consecutive trials was calculated.

During the turning grid test, mice were placed on a grid which was turned upside down. The time hanging was measured with a maximum of 60 s. The average of three consecutive trails was calculated for each mouse. The number of times the mouse was able to climb back on top of the grid was counted during 5 min. Prior to testing, the mice received a 1-min training session.

The sensory behaviour was assessed using an automated Von Frey test (IITC Life Science). After an acclimatization period, the applied force against the hind paw footpad necessary to elicit a reaction from the mouse (retracting paw or flicking) was measured five times on the left and right hind paw.

Electrophysiology

For the nerve conduction measurements, mice were anaesthetized using 1% isoflurane/O_2 gas inhalation and placed on a heating pad to maintain body temperature. Using subdermal needle electrodes (Technomed Europe) and a Medelec Syngery EMG monitor (Vickers Medical) compatible with Synergy software (version 20.1.0.100), the compound muscle action potentials (CMAPs) were assessed by supramaximal stimulation [1 pulse per second (pps), 0.1 ms stimulus duration] at the level of the sciatic notch and recording at the gastrocnemius muscle. Sensory nerve action potentials (SNAPs) were recorded by supramaximal stimulation (6 pps, 0.1 ms stimulus duration) at the distal tip of the tail and were measured 4 cm proximal in the tail. For SNAP recordings, multiple traces were averaged (Leandri *et al.*, 2012). All testing was performed in a blinded manner.

Axonal transport measurements

Prior to the measurements, the cultured DRG neurons were loaded with MitoTracker® Red FM (50 nM, Thermo Fisher Scientific). To visualize the mitochondria, the MitoTracker® Red FM was excited at 580 nm using a TILL Poly V light source. During the measurements, the DRG neurons were perfused in a HEPES solution (containing 148 mM NaCl, 5 mM KCl, 0.1 mM $MgCl_2$, 10 mM glucose, 10 mM HEPES, 2 mM $CaCl_2$) at 37°C by a heath-gravity fed perfusion system and 200 images were recorded at 1 Hz by a cooled CCD camera using TILL VisION. To analyse different parameters of mitochondrial movement, spatio-temporal maps (kymographs) were obtained in Igor Pro (Wavemetrics) using custom-written routines (d'Ydewalle *et al.*, 2011) based on a previous described analysis algorithm (Vanden Berghe *et al.*, 2004). All experiments were performed in a blinded manner. Analysis of the axonal transport measurements were done blinded by encoding the video files that were recorded for each neuron.

Neuromuscular junctions

Prior to dissection, the mice were euthanized by CO_2 inhalation and subsequent cervical dislocation. The gastrocnemius muscle was dissected and snap-frozen in liquid nitrogen-cooled isopentane. Cryosections (20 µm) were fixed with 4% PFA during 10 min and rinsed with PBS. The tissue was permeabilized using PBS-1% Triton™ X-100 for 30 min. Non-specific binding was blocked using 5% normal donkey serum (Sigma-Aldrich) dissolved in PBS-0.3% Triton™ X-100. Antibodies, visualizing nerve axons [anti-neurofilament light chain antibody (Alexa Fluor® 488 conjugated, Cell Signaling, 8024S, 1/500)], the presynapse (anti-SV2A, Developmental Studies Hybridoma Bank, 1/100) and the neuromuscular endplate [α-bungarotoxin (Alexa Fluor®555-conjugated, Life Technologies, B35451, 1/5000)] were dissolved in blocking solution and incubated overnight. Representative confocal images were obtained on a Leica TCS SP8 confocal laser scanning microscope (Leica Microsystems). A minimum of 100 neuromuscular junctions were analysed for innervation per biopsy and samples of $n = 3$ mice were used per treatment condition. *Z*-stacks were acquired using the Leica Application Suite X software (LAS X 3.3.0, Leica Microsystems) and maximum intensity projections images were generated in Fiji (NIH) from 10 plane *Z*-stacks through a 20-µm thick section. All analyses were performed in a blinded manner.

Statistics

All statistical analyses were performed using GraphPad Prism software version 6 (GraphPad software Inc). Unpaired two-tailed Student's *t*-test was used for the comparison of two means. One-way and two-way ANOVA for the multiple group analysis. Data were tested for equal variances using Bartlett's test, Brown-Forsythe test, F-test. Kruskal-Wallis and Mann-Witney were used when no equal variances were obtained in the data sets. $*P < 0.05$, $**P < 0.01$, $***P < 0.0001$. No statistical methods were used to predetermine sample sizes, but our sample sizes are similar to those reported previously (d'Ydewalle *et al.*, 2011).

Results

Selective HDAC6 inhibition blocks GlyRS-HDAC6 interaction

Gene tagging using bacterial artificial chromosomes, protein localization and tandem-affinity purification-mass spectrometry previously identified 100 protein complexes implicated in mitosis including a complex containing HDAC6 and GlyRS (Hutchins *et al.*, 2010). To investigate whether GlyRS and HDAC6 interact, we performed a co-immunoprecipitation assay in N2a cells. Plasmids containing DDK-tagged human GlyRS protein and dsRed-tagged human HDAC6 protein were transiently expressed in N2a cells and pulldown of GlyRS using the DDK-tag resulted in co-immunoprecipitation of HDAC6 (Fig. 1A). Interestingly, this GlyRS-HDAC6 interaction was blocked in cells treated with a selective HDAC6 inhibitor, tubastatin A (Butler *et al.*, 2010), prior to co-immunoprecipitation. In total cell lysate, the acetylation of α-tubulin (Fig. 1A) was enhanced by tubastatin A. As the goal of this study was to investigate whether the therapeutic potential could be further extended to mutant *GARS*-induced CMT, we wanted to assess whether HDAC6 also interacte with mutant GlyRS. As further experiments are performed in the C201R mutant *Gars* mouse model for CMT2D, we chose to work with the human variant (C175R) of the C201R mutation in our mouse model. DDK-tag pulldown of either wild-type or C175R mutant GlyRS resulted in co-immunoprecipitation of HDAC6 (Fig. 1B). However, we could not observe co-immunoprecipitation of the endogenous mouse HDAC6 protein, probably because the HDAC6-GlyRS is a relative weak interaction (Fig. 1B). Additionally, we could observe an altered interaction when GlyRS was mutated.

RNA interference-mediated knock down of GlyRS affects HDAC6 expression

Further assessing this HDAC6-GlyRS interaction on the protein expression level, we treated N2a cells with small interfering RNA (siRNA) to transiently decrease the expression of GlyRS (Fig. 2A). Quantitative PCR at different time points demonstrated a more than 70% reduction in *Gars* mRNA using different siRNA molecules (Supplementary

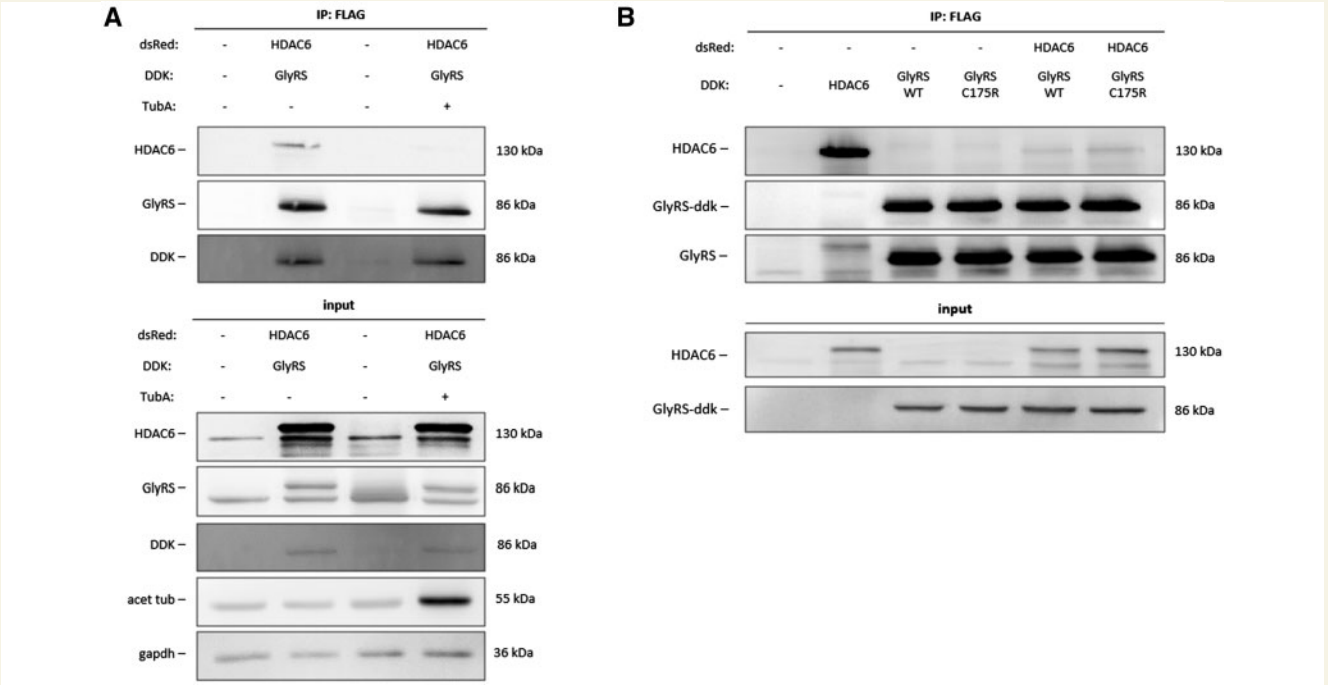

Figure 1 HDAC6 co-immunoprecipitates with GlyRS. (**A**) N2a cells were transiently transfected with either pCMV-DDK-tagged human cDNA encoding GlyRS or pCMV-dsRed-tagged human cDNA encoding HDAC6. Co-immunoprecipitation was performed using agarose beads conjugated to an antibody directed against the DDK peptide. Transfected N2a cells were pre-treated with 1 μM tubastatin A (TubA) or vehicle (DMSO). Western blot analysis was performed to check for equal protein expression and co-immunoprecipitation of HDAC6. (**B**) N2a cells were transiently transfected with either pCMV-DDK-tagged human cDNA encoding wild-type or C175R mutant GlyRS or pCMV-dsRed-tagged human cDNA encoding HDAC6. Co-immunoprecipitation was performed using agarose beads conjugated to an antibody directed against the DDK peptide. Transfected N2a cells were pretreated with 1 μM tubastatin A or vehicle (DMSO). Western blot analysis was performed to check for equal protein expression and co-immunoprecipitation of HDAC6.

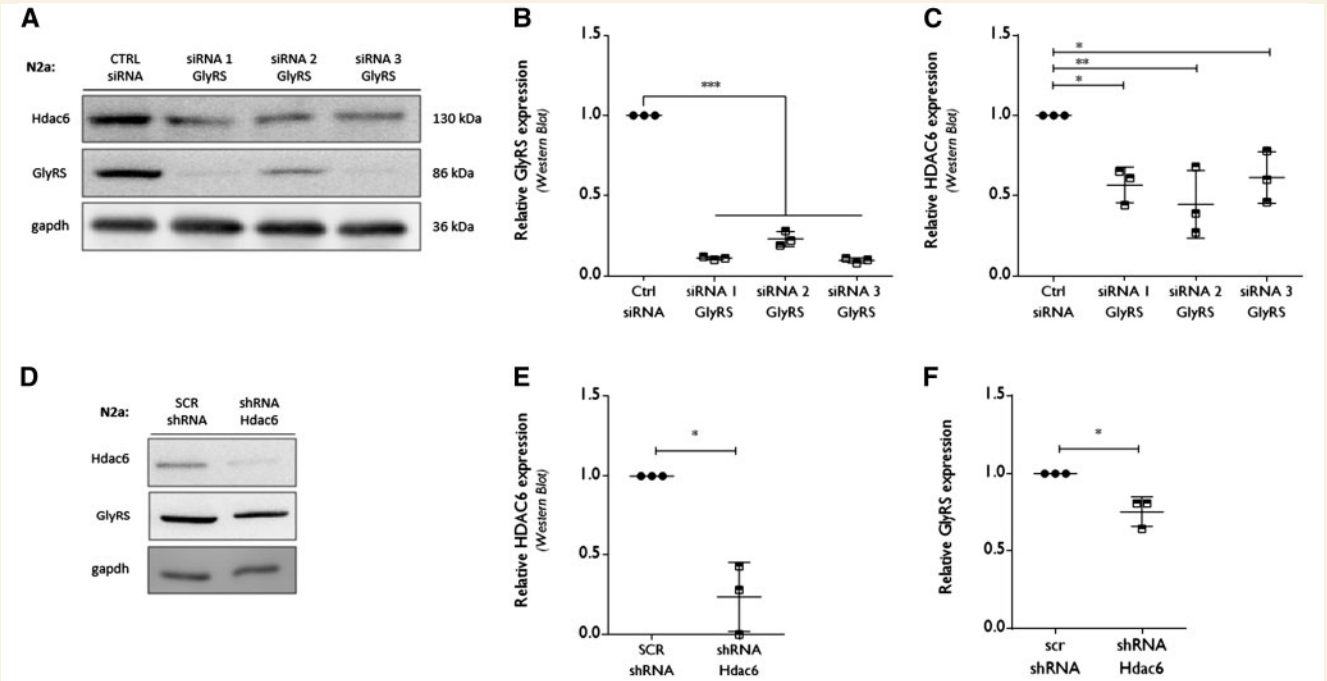

Figure 2 RNA interference-mediated knock down of GlyRS affects HDAC6 expression. (**A**) N2a cells were transfected with siRNA molecules directed against *Gars* (GlyRS) mRNA or a control siRNA. At 72 h post transfection, cells were collected to check protein expression levels by western blot analysis. GAPDH was used as a loading control. (**B**) Using densitometry, the GlyRS protein expression level was determined, relative to GAPDH. All values were normalized to control siRNA samples within each experiment: control siRNA 1.00 ± 0.00, $n = 3$ versus siRNA 1 GlyRS 0.11 ± 0.01, $n = 3$ versus siRNA 2 GlyRS 0.23 ± 0.05, $n = 3$ versus siRNA 3 GlyRS 0.09 ± 0.02; one-way ANOVA, $F(3,8) = 1.935$, $P < 0.0001$. (**C**) The HDAC6 expression levels were analysed using densitometry, relative to the gapdh expression levels and normalized to control siRNA values: control siRNA 1.0 ± 0, $n = 3$ versus siRNA 1 GlyRS 0.57 ± 0.11, $n = 3$ and siRNA 2 GlyRS 0. 45 ± 0.21, $n = 3$ and siRNA 3 GlyRS 0.61 ± 0.16, $n = 3$; One-way ANOVA, $F(3,8) = 8.327$, $P = 0.0076$; Dunnett's multiple comparisons test. (**D**) pCMV-dsRed plasmids containing either a scrambled shRNA or short hairpin RNA (shRNA) directed against *Hdac6* mRNA were transfected in N2a cells. At 72 h post transfection, cells were collected to check protein expression levels by western blot analysis. (**E**) HDAC6 expression was checked by western blot analysis after 72 h shRNA-mediated knockdown. Densitometry was used to calculate HDAC6 expression levels, relative to GAPDH and all values were normalized to scrambled (SCR) shRNA samples: scrambled shRNA 1.00 ± 0.00, $n = 3$ versus shRNA *Hdac6* 0.24 ± 0.22, $n = 3$; one-sample *t*-test, $t = 6.088$, $P = 0.0259$. (**F**) The relative GlyRS expression levels were calculated using densitometry, relative to GAPDH levels and normalized to scrambled shRNA values: scrambled shRNA 1.0 ± 0.0, $n = 3$ versus shRNA *Hdac6* 0.75 ± 0.09, $n = 3$; one sample *t*-test, $t = 4.353$, $P = 0.0489$.

Fig. 1A). Western blot analysis confirmed the siRNA-mediated reduction in GlyRS at 72 h post transfection (Fig. 2A and B). Reduced *Gars*/GlyRS expression resulted in decreased levels of HDAC6 only at the protein level (Fig. 2A and C) as mRNA levels remained unaltered (Supplementary Fig. 1B). Conversely, transient knock-down of HDAC6 using shRNA resulted in reduced expression of HDAC6 both at the mRNA (Supplementary Fig. 1C) and at the protein level (Fig. 2D and E). Interestingly, this resulted in a reduction of GlyRS protein (Fig. 2D and F), while quantitative PCR analysis showed a trend towards upregulated GlyRS expression (Supplementary Fig. 1D). The latter effect could be a compensatory mechanism in response to the reduced protein levels of GlyRS. All together, these data indicate that GlyRS and HDAC6 are necessary to stabilize each other at the protein expression level.

Mutant *Gars* causes motor and sensory problems in a mouse model of CMT2D

First, we confirmed the motor and sensory problems that develop with age and that are caused by the expression of an *N*-ethyl-*N*-nitrosourea (ENU)-induced mutant (C201R) GlyRS (Achilli *et al.*, 2009). $Gars^{C201R/+}$ mice develop symptoms from early age on as shown by decreased body weight and reduced performance on an accelerating rotarod (Supplementary Fig. 2A and B, and Fig. 3A). Grip strength measured in all paws using a grid (Fig. 3B) or only in the forepaws with a triangular bar (Supplementary Fig. 2C) was severely reduced in $Gars^{C201R/+}$ mice indicative of clear muscle weakness. $Gars^{C201R/+}$ mice also failed on the hanging wire test in which mice have to hold on to a grid during a 60-s period (Fig. 3C).

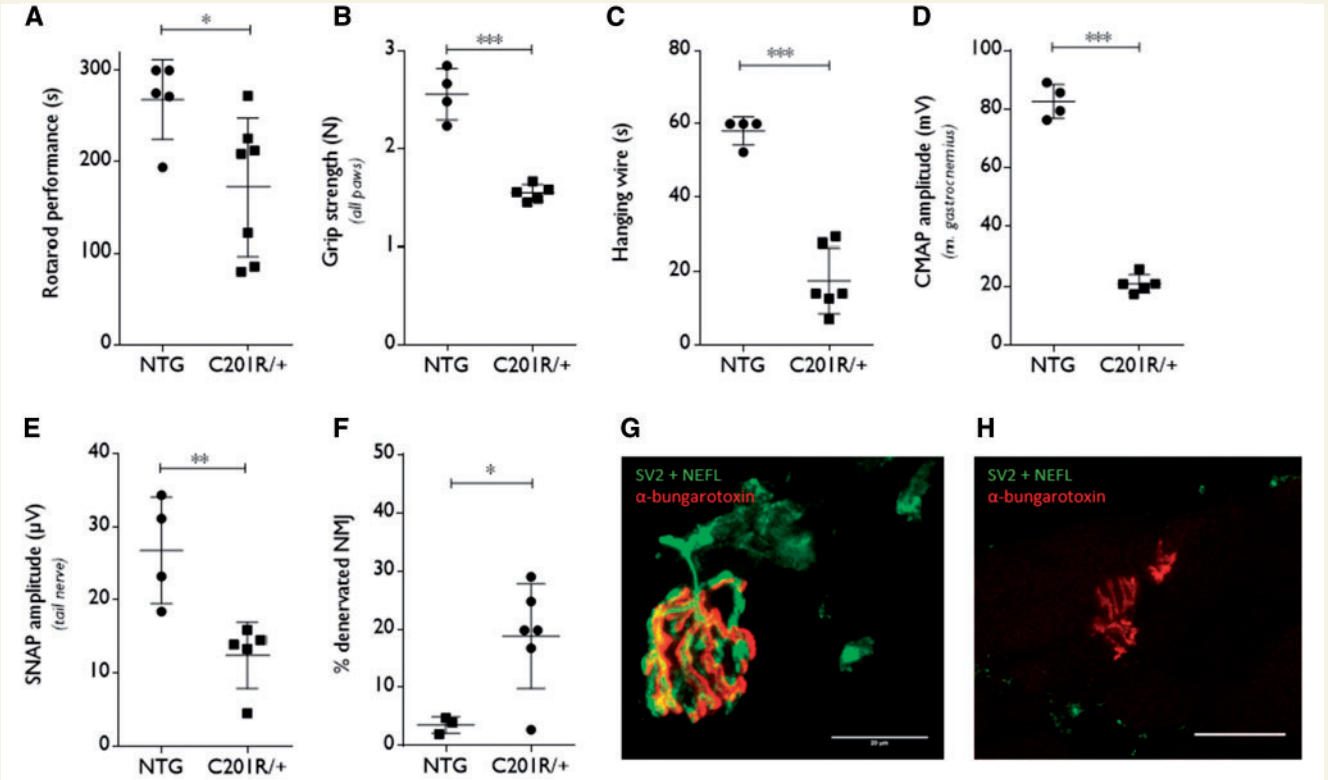

Figure 3 Motor and sensory deficits reminiscent of CMT2D are present in 1-year old *Gars*$^{C201R/+}$ mice. (**A**) The motor performance of *Gars*$^{C201R/+}$ mice and littermate controls (non-transgenic, NTG) was assessed by a rotarod test which accelerates from 4 to 40 rpm for 5 min: non-transgenic 268 ± 43.68 s, $n = 5$ mice versus *Gars*$^{C201R/+}$ 172 ± 75.51 s, $n = 7$ mice; unpaired *t*-test t = 2.531, $P = 0.0298$. **B.** Grip strength was measured in all paws using a grid in combination with a dynamometer: non-transgenic 2.55 ± 0.26 N, $n = 4$ mice versus *Gars*$^{C201R/+}$ 1.54 ± 0.08 N, $n = 5$ mice; unpaired *t*-test t = 8.211, $P < 0.0001$. (**C**) Mice were tested for the ability to hold on to a grid in the hanging wire test and the time spent hanging was measured with a maximum time limit of 60 s: non-transgenic 58.08 ± 3.84 s, $n = 4$ mice versus *Gars*$^{C201R/+}$ 17.45 ± 8.96 s, $n = 6$ mice; unpaired *t*-test t = 8.436, $P < 0.0001$. (**D**) CMAP amplitudes were recorded in the gastrocnemius muscle: non-transgenic 82.68 ± 5.79 mV, $n = 4$ mice versus *Gars*$^{C201R/+}$ 20.84 ± 3.14 mV, $n = 5$ mice; unpaired *t*-test t = 20.61, $P < 0.0001$. (**E**) SNAP amplitudes were measured in the tail nerve: non-transgenic 26.75 ± 7.263 μV, $n = 4$ mice versus *Gars*$^{C201R/+}$ 12.42 ± 4.53 μV, $n = 5$ mice; unpaired *t*-test t = 3.645, $P = 0.0082$. (**F**) The innervation of neuromuscular junctions was evaluated by quantifying the percentage of neuromuscular junctions demonstrating overlap of neurofilament light, NEFL/synaptic vesicle glycoprotein 2A, SV2 and α-bungarotoxin staining: non-transgenic 3.57 ± 1.43%, $n = 3$ mice versus *Gars*$^{C201R/+}$ 18.81 ± 8.98 %, $n = 6$ mice; unpaired *t*-test t = 2.826, $P = 0.0255$. (**G** and **H**) Innervated (**G**) and denervated (**H**) neuromuscular junctions (NMJs) in the gastrocnemius muscle were visualized by immunofluorescence (green: NEFL + SV2; red: α-bungarotoxin). Confocal images are represented. Scale bar = 20 μm. For colour blind corrected figure, see Supplementary Fig. 2F and G.

Nerve conduction measurements showed significantly reduced CMAP amplitudes in the sciatic nerve (Fig. 3D) and significantly reduced SNAP amplitudes in the tail nerve (Fig. 3E), demonstrating motor and sensory axonal loss. The latencies of both the CMAPs and SNAPs were increased (Supplementary Fig. 2D and E), which could be due to the loss of the largest myelinated axons.

We also performed histopathology on the gastrocnemius muscle and visualized the neuromuscular junctions and the level of innervation. The neuromuscular junctions from *Gars*$^{C201R/+}$ mice appeared dysmorphic (Fig. 3G and H) and the number of innervated neuromuscular junctions was significantly reduced (Fig. 3F).

Acetylated α-tubulin levels are decreased in peripheral nervous tissue of *Gars*$^{C201R/+}$ mice

As we obtained evidence for a molecular link between GlyRS and HDAC6, we determined the acetylation levels of α-tubulin in spinal cord and sciatic nerve tissue from *Gars*$^{C201R/+}$ mice at the age of 1 year. In sciatic nerve tissue, the acetylation of α-tubulin was significantly decreased relative to total α-tubulin levels in mice expressing GlyRS$^{C201R/+}$ (Fig. 4A and B). In spinal cord, the acetylation of α-tubulin was unaltered (Fig. 4C and D). As acetylation of α-tubulin plays an important role in the

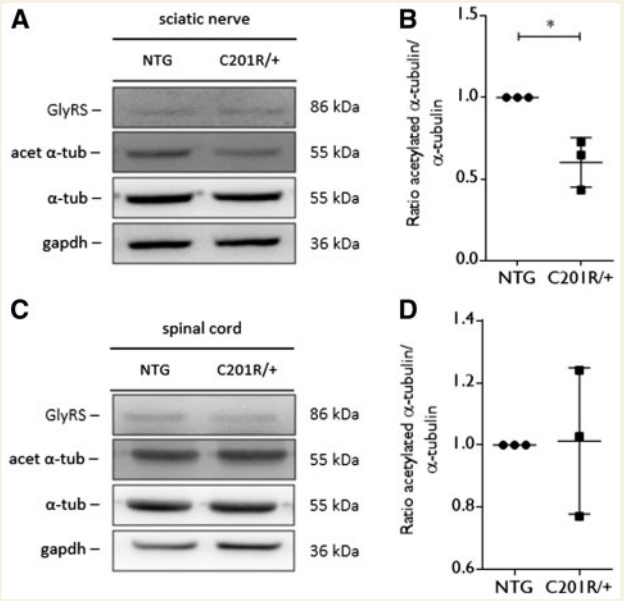

Figure 4 Acetylated α-tubulin levels are altered in peripheral nerve tissue from *Gars*$^{C201R/+}$ mice. (**A**) Western blot analysis was used to determine the acetylation status of α-tubulin in tissue homogenates from *Gars*$^{C201R/+}$ and littermate control mice (non-transgenic, NTG). An antibody directed against GlyRS was used to assess GlyRS expression levels. GAPDH expression levels were used as a control for equal sample loading. (**B**) The amount of acetylated α-tubulin compared to the total α-tubulin levels was quantified by densitometry and the values were normalized to the non-transgenic samples: non-transgenic 1.00 ± 0.00, $n = 3$ samples versus *Gars*$^{C201R/+}$ 0.60 ± 0.15 ms, $n = 3$ samples; unpaired *t*-test: $t = 4.518$, $P = 0.0107$. (**C**) The level of acetylated α-tubulin was detected by western blot analysis in tissue homogenates from spinal cord from *Gars*$^{C201R/+}$ and littermate control (non-transgenic) mice. GlyRS expression levels were checked and GAPDH was used as a loading control. (**D**) The ratio between acetylated α-tubulin and total α-tubulin was quantified by densitometry and values were normalized to non-transgenic samples. $n = 3$ mice.

axonal trafficking of cellular cargoes, we wanted to assess the mitochondrial movement in primary DRG neuron cultures from adult *Gars*$^{C201R/+}$ and non-transgenic littermate control mice. First, we analysed the acetylated α-tubulin levels in DRGs isolated from *Gars*$^{C201R/+}$ mice. We found significantly decreased acetylated α-tubulin levels as compared to littermate controls (Fig. 5A and B).

Mitochondrial transport is disrupted in dorsal root ganglion cultures from *Gars*$^{C201R/+}$ mice

Next, we cultured DRG neurons from adult *Gars*$^{C201R/+}$ and non-transgenic littermate control mice to study the effect of mutant GlyRS on the sensory phenotype of *Gars*$^{C201R/+}$ mice. The DRG neurons were visualized using immunofluorescence, showing expression of GlyRS in both non-transgenic and in *Gars*$^{C201R/+}$ cells (Supplementary Fig. 3A and B). Based on β3-tubulin signal length, decreased neurite outgrowth was observed in *Gars*$^{C201R/+}$ DRG neurons (Supplementary Fig. 3C–E). However, assessing cell viability using an luminescence-based assay monitoring the ATP concentration (ATPlite) and a fluorescence-based assay measuring hydrolysis of fluorochrome 4-methylumbelliferyl heptanoate (MUH) by the intracellular esterases (MUH assay) showed no alteration in cell viability between non-transgenic and *Gars*$^{C201R/+}$ DRG neuron cultures (Supplementary Fig. 4A and B).

Mitochondrial dynamics are important in neurons, especially in peripheral nerve axons as these axons have high energy demands due to their long lengths. Disturbances in axonal mitochondrial transport are often associated with peripheral neuropathies (Pareyson *et al.*, 2015). Therefore, we performed live cell imaging of mitochondrial movement along the neurites of cultured DRG neurons from adult *Gars*$^{C201R/+}$ or non-transgenic mice. Analysis of the kymographs showed a reduced percentage of moving (Fig. 5C and D) and an increased fraction of stationary mitochondria (Fig. 5C and F) in the neurites of *Gars*$^{C201R/+}$ DRG neurons. Detailed analysis of the mitochondrial movement showed that both anterograde and retrograde dynamics were affected (Fig. 5E).

Considering that acetylated α-tubulin is important for the process of mitochondrial axonal transport, we treated the *Gars*$^{C201R/+}$ DRG neuron cultures with the selective HDAC6 inhibitor, tubastatin A. This treatment increased retrograde movement and normalized the overall percentage of moving and stationary mitochondria (Fig. 5D–F). Immunocytochemistry confirmed that tubastatin A treatment indeed increased acetylated α-tubulin levels in the *Gars*$^{C201R/+}$ DRG neuron cultures (Fig. 5G and H). Additionally, tubastatin A treatment did not alter cell viability of the DRG neuron cultures (Supplementary Fig. 4A and B).

As the motor phenotype is generally more pronounced in CMT patients, we investigated the axonal transport movement of mitochondria in primary motor neurons cultures. The motor neurons were cultured from *Gars*$^{C201R/+}$ and non-transgenic embryo's (embryonic Day 13.5) as it was technically not possible to culture adult primary motor neurons. In these cultured motor neurons we could detect GlyRS expression by immunofluorescence (Supplementary Fig. 5A and B). Although a trend towards decreased mitochondrial transport was observed, no significant change in the number of moving or stationary mitochondria was quantified, nor in the total number of mitochondria (Supplementary Fig. 5C–E). We also assessed acetylation of α-tubulin in brain tissue of embryonic Day 13.5 embryos as defects in motor and sensory nerve axons seem to arise at an early age (Sleigh *et al.*, 2014, 2017). However, no difference in acetylated α-tubulin was detected by western blot while GlyRS was already expressed at this stage (Supplementary Fig. 6A and B).

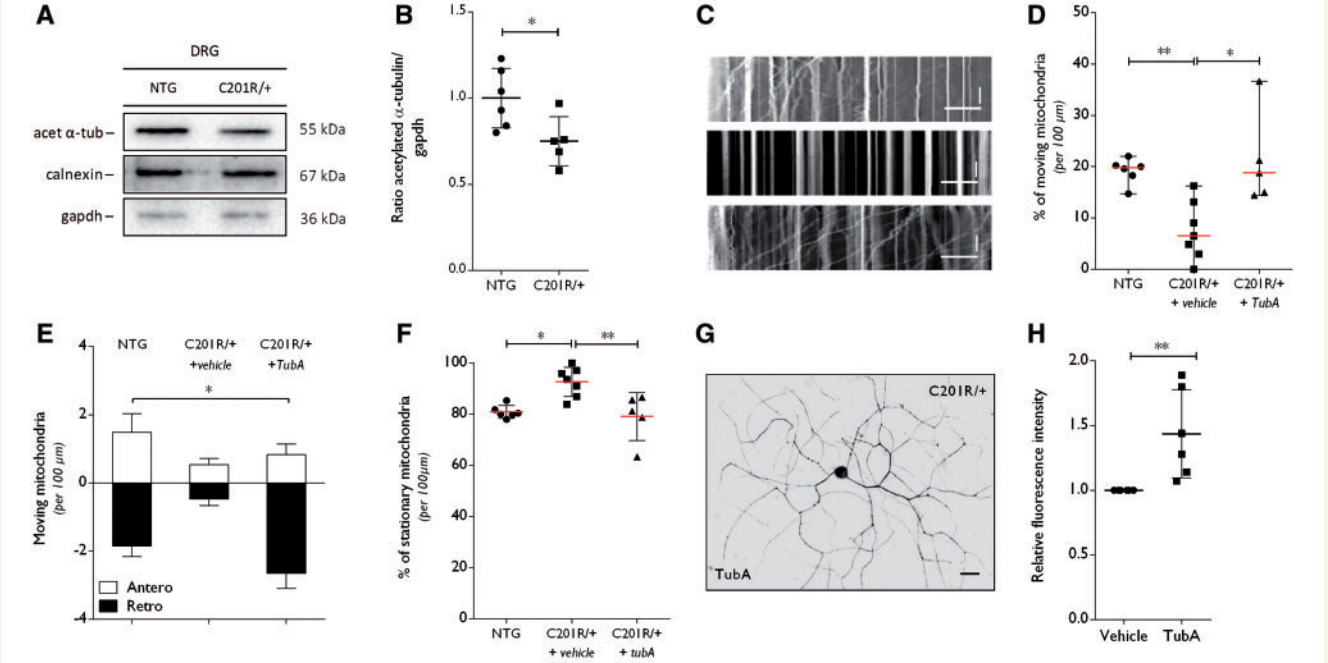

Figure 5 Altered α-tubulin acetylation and disturbances in mitochondrial axonal transport in DRGs from *Gars*$^{C201R/+}$ mice are rescued by selective HDAC6 inhibition. (**A**) Western blot analysis was used to determine the acetylation status of α-tubulin in DRG homogenates from *Gars*$^{C201R/+}$ and littermate control mice (non-transgenic, NTG). GAPDH and calnexin were used as loading control. (**B**) Densitometry was used to quantify the ratio of acetylated α-tubulin to GAPDH levels. Values were normalized to non-transgenic samples. Non-transgenic 1.00 ± 0.17, $n = 6$ mice versus *Gars*$^{C201R/+}$ 0.75 ± 0.14, $n = 5$ mice; unpaired *t*-test t = 2.574, $P = 0.0300$. (**C**) Representative kymographs from the analysis of mitochondrial movement in non-transgenic (*top*) and *Gars*$^{C201R/+}$ (*middle* and *bottom*) DRG neurons. Stationary mitochondria are represented by vertical lines. Lines deflecting to the right or left are anterograde or retrograde moving mitochondria, respectively. Horizontal scale bar = 30 µm. Vertical scale bar = 80 s. DRG neurons were treated with vehicle or 1 µM tubastatin A (TubA). (**D**) Mitochondrial movement was quantified within one neurite per cell, relative to the total number of mitochondria per 100 µm. *Gars*$^{C201R/+}$ DRG neurons were treated with vehicle or with 1 µm tubastatin A (TubA): non-transgenic 19.14 ± 2.48% moving mitochondria, $n = 6$ different DRG primary cultures versus *Gars*$^{C201R/+}$ + vehicle 7.53 ± 5.69% moving mitochondria, $n = 7$ different DRG primary cultures versus *Gars*$^{C201R/+}$ + tubastatin A 21.21 ± 9.07% moving mitochondria, $n = 5$ different DRG primary cultures; Kruskal-Wallis test, $P = 0.0015$. (**E**) Anterograde and retrograde moving mitochondria were quantified from the kymographs obtained from non-transgenic, vehicle-treated and tubastatin A-treated *Gars*$^{C201R/+}$ DRG neurons: antero 0.95 ± 0.46 mitochondria, $n = 3$ versus retro −1.66 ± 1.10 mitochondria, $n = 3$ different DRG primary cultures; two-way ANOVA, treatment $F(2,18) = 3.898$, $P = 0.0392$, direction of transport $F(1,18) = 81.20$, $P < 0.0001$. (**F**) The number of stationary mitochondria in the neurites from non-transgenic or *Gars*$^{C201R/+}$ DRG neurons was quantified relative to the total number of mitochondria, in the absence or presence of tubastatin A was assessed. Non-transgenic 80.87 ± 2.48% stationary mitochondria, $n = 6$ different DRG primary cultures versus *Gars*$^{C201R/+}$ + vehicle 92.57 ± 5.75% stationary mitochondria, $n = 7$ different DRG primary cultures versus *Gars*$^{C201R/+}$ + tubastatin A 79.09 ± 9.34, $n = 5$ different DRG primary cultures; one-way ANOVA, $F(2,15) = 1.515$, $P = 0.0030$. (**G**) The acetylation of α-tubulin was determined by immunocytochemistry in *Gars*$^{C201R/+}$ DRG neuron cultures on tubastatin A treatment. (**H**) Quantification of the intensity of acetylated α-tubulin in neurites of DRG neuron cultures normalized to the fluorescence length: *Gars*$^{C201R/+}$ + vehicle 1.00 ± 0.0, $n = 6$ different DRG primary cultures versus *Gars*$^{C201R/+}$ + tubastatin A 1.44 ± 0.34, $n = 6$ cells from six different DRG primary cultures; Mann-Whitney test, $P = 0.0022$.

Inhibition of HDAC6 improves motor and sensory deficits in *Gars*$^{C201R/+}$ mice

To investigate whether HDAC6 inhibition could improve the motor and sensory deficits of *Gars*$^{C201R/+}$ mice, tubastatin A was administered through daily intraperitoneal injections in 4-month-old mutant mice. After the treatment period, motor behaviour and nerve conduction parameters were evaluated. Tubastatin A treated *Gars*$^{C201R/+}$ mice showed a significant improvement in grip strength (Fig. 6A) and performed slightly better on the accelerating rotarod (Fig. 6B). There was no altered performance in the hanging wire test, although the number of attempts to climb back on top of the platform was significantly improved after treatment (Fig. 6C). Tubastatin A treatment also significantly increased the CMAP amplitudes (Fig. 6D), indicating regeneration of motor nerve axons in the sciatic nerve. Moreover, the SNAP amplitudes were significantly increased by inhibiting the deacetylating function of HDAC6 (Fig. 6E). Treatment of littermate control mice with tubastatin A did not alter the nerve

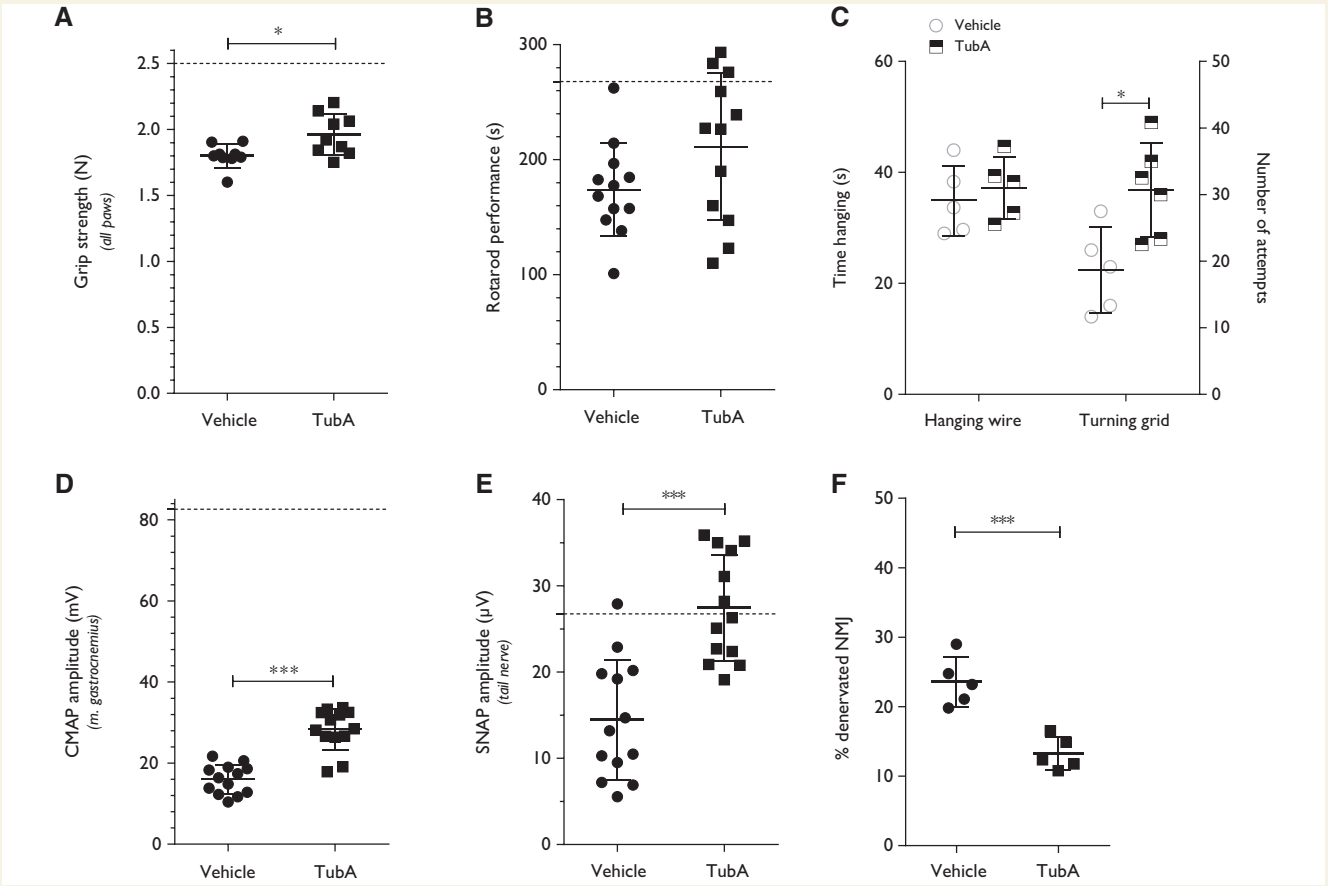

Figure 6 Treatment of *Gars*$^{C201R/+}$ mice with a HDAC6 inhibitor improves motor behaviour and stimulates regeneration of motor and sensory nerves in 4-month-old mice. (**A**) After daily intraperitoneal injections during 40 consecutive days with tubastatin A (50 mg/kg), the grip strength in all paws of vehicle- versus tubastatin A-treated *Gars*$^{C201R/+}$ mice was assessed: vehicle 1.80 ± 0.09 N, *n* = 9 mice versus tubastatin A 1.96 ± 0.16 N, *n* = 12 mice; unpaired *t*-test: t = 2.697, *P* = 0.0159. (**B**) The motor behaviour after treatment was measured by the accelerated rotarod test: vehicle 174 ± 40.47 s, *n* = 12 mice versus tubastatin A 211 ± 63.96 s, *n* = 12 mice; unpaired *t*-test: t = 1.706, *P* = 0.1021. (**C**) The time spent hanging (hanging wire) as well as the number of attempts to climb back on top of a grid (turning grid) was measured in vehicle versus tubastatin A-treated mice: turning grid test: vehicle 22.40 ± 7.70, *n* = 5 mice versus tubastatin A 36.83 ± 8.42, *n* = 5 mice; unpaired *t*-test t = 2.939, *P* = 0.0165. (**D**) The CMAP amplitudes were measured in the sciatic nerve in vehicle and tubastatin A-treated mice: vehicle 15.98 ± 3.61 mV, *n* = 13 mice versus tubastatin A 28.28 ± 5.09 mV, *n* = 13 mice; unpaired *t*-test t = 7.110, *P* < 0.0001. (**E**) SNAP amplitudes were measured in the tail nerve in vehicle and tubastatin A-treated mice: vehicle 14.45 ± 6.98 µV, *n* = 13 mice versus tubastatin A 27.45 ± 6.18 µV, *n* = 13 mice; unpaired *t*-test t = 5.027, *P* < 0.0001. (**F**) Quantification of the percentage of innervated neuromuscular junctions (NMJs) in the gastrocnemius muscle after treatment: vehicle 23.57 ± 3.58%, *n* = 5 mice (one muscle per mouse) versus tubastatin A 13.27 ± 2.38 %, *n* = 5 mice (one muscle per mouse); unpaired *t*-test t = 5.366, *P* = 0.0007.

conduction of littermate control mice (Supplementary Fig. 7A–D).

After the treatment period, the mice were sacrificed and histopathology was performed to check the innervation of the neuromuscular junctions as well as the levels of acetylated α-tubulin. We found enhanced reinnervation of the gastrocnemius muscle by comparing the number of innervated neuromuscular junctions in vehicle- and tubastatin A-treated mice (Fig. 6F). On western blot, we also detected an increased level of acetylated α-tubulin in sciatic nerve and DRGs homogenates after treatment with tubastatin A (Fig. 7A, B, D and E). Acetylation of α-tubulin in spinal cord remained unaltered (Fig. 7C and F).

Altogether, these data indicate that selective HDAC6 inhibition improved motor and sensory defects, which correlated with an increased innervation and a higher α-tubulin acetylation.

Discussion

The genetic heterogeneity among CMT patients hampers the identification of potential common therapeutic targets in preclinical research. In this study, we demonstrated reduced levels of acetylated α-tubulin in peripheral nerves and DRGs of a mutant *Gars*-induced CMT2 mouse model.

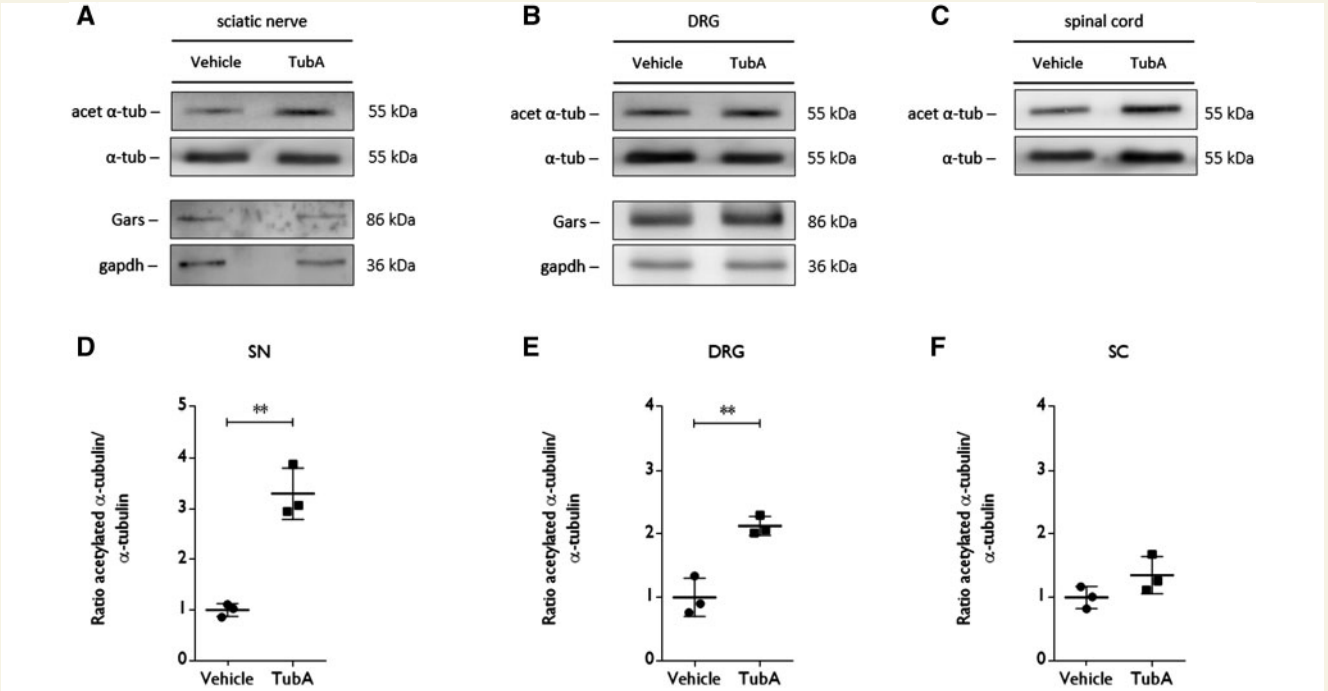

Figure 7 Tubastatin A treatment increases the acetylation of α-tubulin in sciatic nerve and DRG homogenates from *Gars*$^{C201R/+}$ mice. (**A** and **D**) The levels of acetylated of α-tubulin and *Gars* expression in sciatic nerve homogenates was determined by western blot. Densitometry was used to assess the ratio of acetylation α-tubulin to total α-tubulin levels in sample from vehicle and tubastatin A-treated mice. All values were normalized to samples from vehicle treated mice: vehicle 1.00 ± 0.18, $n = 3$ mice versus tubastatin A 1.35 ± 0.29, $n = 3$ mice; unpaired *t*-test t = 7.636, $P = 0.0016$. (**B** and **E**) The acetylation status of α-tubulin and *Gars* expression in DRGs from vehicle- and tubastatin A-treated mice was determined using western blot. The ratio between the acetylation of α-tubulin and total α-tubulin levels was quantified by densitometry. All values were normalized to samples from vehicle-treated mice: vehicle 1.00 ± 0.30, $n = 3$ mice versus tubastatin A 2.13 ± 0.15, $n = 3$ mice; unpaired *t*-test t = 5.799, $P = 0.0044$. (**C** and **F**) Spinal cord samples were collected from vehicle- and tubastatin A-treated mice to assess the acetylation status of α-tubulin. Densitometry was used to quantify the ratio between acetylated and total α-tubulin levels. All values were normalized to samples from vehicle-treated mice: vehicle 1.00 ± 0.18, $n = 3$ mice versus tubastatin A 1.35 ± 0.29, $n = 3$ mice; unpaired *t*-test t = 1.8, $P = 0.1463$.

Furthermore, we demonstrated that mutant *Gars* affects neurite length and axonal transport in primary neurons, and that treatment with a specific HDAC6 inhibitor restored these axonal defects. Systemic delivery of this HDAC6 inhibitor partially restored motor and sensory nerve conduction defects, increased muscle innervation and improved motor behaviour. Our study suggests that reduced acetylated α-tubulin levels in peripheral nerves may represent a common pathogenic hallmark of CMT2, and highlights the potential of HDAC6 inhibitors as therapeutic strategy for peripheral neuropathies.

To study the effects of HDAC6 inhibition in CMT2D, we used the previously established mouse model carrying an endogenous C201R mutation in *Gars* (Achilli *et al.*, 2009). Further characterization of these mice by nerve conduction studies demonstrated a 75% lower CMAP amplitude measured in the gastrocnemius muscle (after stimulation of the sciatic nerve) of *Gars*$^{C201R/+}$ mice in comparison to littermate controls of the same age. This seems to be in contradiction with the 15% neuromuscular junctions denervation observed in the *Gars*$^{C201R/+}$ mice. However, our immunofluorescence technique only assesses the percentage of innervated neuromuscular junctions in the remaining motor endplates and does not reflect the potential loss of total number of functional motor units. The 80% decrease in CMAP amplitude and the lower muscle mass (gastrocnemius muscle) observed in C201R mutant mice suggests a decrease in the total number of motor units and that the remaining units are chronically de- and reinnervated (Lewis *et al.*, 2003). The reduced CMAP and SNAP latencies indicated slower nerve conduction velocities and thus the occurrence of dysmyelination. However, we and others (Achilli *et al.*, 2009) did not observe any defect of sciatic nerve axon myelination in this mouse model. Therefore, the increase in latencies of CMAPs and SNAPs is most likely due to the loss of the largest myelinated axons, which determine the nerve conduction velocity.

Pharmacological inhibition of HDAC6 ameliorates the phenotype of the *Gars*$^{C201R/+}$ mice although the observed effects are rather limited as compared to the results obtained in mutant *HSPB1*-induced CMT2 mouse model (d'Ydewalle *et al.*, 2011). However, it should be taken into account that the phenotype induced by mutant GlyRS arises already at young age and that the axonal degeneration in motor and sensory nerves, as shown by CMAP and SNAP amplitude recordings, is more severe in

comparison to the mutant *HSPB1* mice (d'Ydewalle *et al.*, 2011). Hence, the mutant *Gars*-induced mouse model has a more pronounced phenotype, which could explain why the effects of HDAC6 inhibition are smaller. Additionally, it is possible that mechanisms, unresponsive to pharmacological HDAC6 inhibition and other than decreased α-tubulin acetylation and axonal transport defects, contribute to the disease phenotype.

The increase in the CMAP and SNAP amplitudes after treatment indicates an enhanced motor and sensory axonal outgrowth. Hence, we could demonstrate ameliorated neuromuscular junction innervation after treatment with a selective HDAC6 inhibitor. This is an interesting outcome as defects in the maturation of neuromuscular junctions were shown to precede the loss of synaptic connectivity of lower motor neurons (Sleigh *et al.*, 2014). Additionally, synaptic deficits at the neuromuscular junctions correlated with impaired neuromuscular performance and disease progression, demonstrating the contribution of neuromuscular junction pathology to the early CMT2D pathology (Spaulding *et al.*, 2016). HDAC6 has been shown to play a role in neurotransmitter release by deacetylating bruchpilot (*brp*) in a *Drosophila* model for TDP-43-induced toxicity (Miskiewicz *et al.*, 2014). Reducing HDAC6 expression levels in TDP-43 expressing flies ameliorated presynaptic density defects as well as adult locomotor problems (Miskiewicz *et al.*, 2014). These results indicate that targeting the acetylation status of HDAC6-associated proteins can also have potential therapeutic effects in neurodegeneration.

Decreased levels of acetylated α-tubulin and axonal transport deficits were present in both mutant *Hspb1* (d'Ydewalle *et al.*, 2011) and mutant *Gars* mice. Decreased acetylation of α-tubulin has also been demonstrated in other neurodegenerative disorders (Van Helleputte *et al.*, 2014). For example, α-tubulin was found to be hypo-acetylated in stroke-induced brain infarction and the recovery after stroke was improved by pharmacological HDAC6 inhibition (Wang *et al.*, 2016). This suggests that HDAC6 could be used as a target in various neurodegenerative disorders associated with reduced α-tubulin acetylation and mitochondrial axonal transport abnormalities. Indeed, axonal trafficking abnormalities observed in motor neurons derived from induced pluripotent stem cells (iPSCs) of CMT2 patients could be rescued by the selective inhibition of HDAC6 (Kim *et al.*, 2016). In the DRG neuron cultures from $Gars^{C201R/+}$ mice, we could show that the mitochondrial axonal transport was affected both in antero- and retrograde directions. HDAC6 inhibition counteracted the axonal transport defects in $Gars^{C201R/+}$ DRG neurons, specifically in the retrograde sense. Interestingly, Kalmar *et al.* (2017) reported abnormal axonal movement of mitochondria in the retrograde direction in primary motor neurons expressing mutant HSPB1 and we previously demonstrated the beneficial effect of HDAC6 inhibition on mitochondrial axonal transport movement (d'Ydewalle *et al.*, 2011). Moreover, studying Parkinson's disease in a mutant LRRK2-expressing *Drosophila* model demonstrated the beneficial effects of reducing HDAC6 expression or administration of trichostatin A on axonal trafficking and locomotor behaviour (Godena *et al.*, 2014).

We demonstrated that HDAC6 co-immunoprecipitated with GlyRS and that this interaction could be blocked by pretreatment with tubastatin A. The interaction of GlyRS with HDAC6 was previously described in a systematic analysis for the identification of protein complexes essential for spindle assembly and chromosome segregation (Hutchins *et al.*, 2010). However, whether these proteins interact directly and how both proteins affect cell-biological function is not yet clear. As decreased levels of acetylated alpha-tubulin were found in our mouse model, indicating enhanced HDAC6 activity, the question remains whether mutant GlyRS can affect HDAC6 function. Alternatively, several forms of bacterial tRNA synthetases have been shown to be prone to post-translational modifications such as acetylation, which is an important regulator of their function or localization (Ye *et al.*, 2017). The intriguing question remains whether eukaryotic GARS can be acetylated and whether this would affect its function.

Interestingly, HSPB1 has also been shown to bind HDAC6 and decreased acetylation of alpha-tubulin was also detected in peripheral nervous tissue of a mutant *HSPB1*-induced CMT2 and distal HMN mouse model (Zhang *et al.*, 2007; d'Ydewalle *et al.*, 2011). Mutant HSPB1 has been shown to possess hyperactive properties as it has an enhanced binding to α-tubulin leading to stabilization of microtubules (Almeida-Souza *et al.*, 2011). Additionally, GlyRS has also been shown to interact with HSPB1 (Wan *et al.*, 2015). Enhanced binding properties have been reported previously for GlyRS mutant proteins (He *et al.*, 2015). Hydrogen-deuterium mass spectrometry demonstrated that mutations cause a conformational opening of the GlyRS structure, leading to a neomorphic surface for pathological interactions (Nangle *et al.*, 2007; Xie *et al.*, 2007). Indeed, GlyRS can bind the neurophilin-1 (Nrp-1) receptor. When mutated, GlyRS obtains an altered conformation and shows enhanced binding to Nrp-1 which in turn disrupts the interaction of Nrp-1 to vascular endothelial growth factor (VEGF). Genetic deletion of Nrp-1 worsens the CMT phenotype of mutant *Gars* mice while expression of VEGF improves the motor problems (He *et al.*, 2015). However, we could not observe a strong enhanced binding of mutated GlyRS-HDAC6 interaction. A more detailed binding analysis is required to detect enhanced binding properties. In summary, these observations could indicate a common pathway leading to mutant HSPB1 and mutant GlyRS-induced pathology.

As there is currently no curative treatment available for CMT2 patients, our study provides important evidence that HDAC6 can serve as a target for a pharmacological therapy for at least two different genetic causes of CMT2. We hypothesize that mutations in CMT2-associated proteins such as HSPB1 and GlyRS may cause hyperactivity of HDAC6 leading to altered acetylation of various HDAC6 substrates, including α-tubulin. This altered acetylation status affects

processes important in neurons such as axonal transport leading to an increased vulnerability of motor and sensory nerve axons. Therefore, developing molecules that act as HDAC6 inhibitors with improved drug-like properties is an important next step in the preclinical research for the development of a new therapy (De Vreese *et al.*, 2015, 2016; Shen *et al.*, 2016; Benoy *et al.*, 2017). Moreover, decreased acetylation of α-tubulin and defects in mitochondrial transport further support the hypothesis that disturbances in cytoskeletal proteins and axonal trafficking are part of a common pathogenic mechanism underlying peripheral neuropathies such as CMT. In conclusion, with this study we further confirm the involvement of HDAC6 in degenerative disorders such as CMT and we hypothesize that HDAC6 could be an important therapeutic target for peripheral neuropathies in general.

Funding

This work was supported by grants from the Fund for Scientific Research Flanders (FWO-Vlaanderen), the Belgian government (Interuniversity Attraction Poles of the Belgian Federal Science Policy Office), the Association Belge contre les Maladies neuro-Musculaires (ABMM), the Muscular Dystrophy Association (MDA), the European Community's Health Seventh Framework Programme (FP7/2007-2013 under grant agreement 259867) and National Institutes of Health [NIH, NS079183]. P.V.D., W.R. and L.V.D.B. are supported by the 'Opening the Future' Fund (KU Leuven). W.R. is supported by the 'E. von Behring Chair for Neuromuscular and Neurodegenerative Disorders'. V.B. and L.V.H. are supported by the 'Agency for Innovation by Science and Technology in Flanders' (IWT-Vlaanderen). R.P. was supported by grants from the Central Remedial Clinic (CRC) Ireland and the National University of Ireland (NUI) and is currently supported by the FWO-Vlaanderen. P.V.D. holds a clinical investigatorship of FWO-Vlaanderen. The authors declare no conflict of interest.

Supplementary material

Supplementary material is available at *Brain* online.

References

Achilli F, Bros-Facer V, Williams HP, Banks GT, AlQatari M, Chia R, et al. An ENU-induced mutation in mouse glycyl-tRNA synthetase (GARS) causes peripheral sensory and motor phenotypes creating a model of Charcot-Marie-Tooth type 2D peripheral neuropathy. Dis Model Mech 2009; 2: 359–73.

Almeida-Souza L, Asselbergh B, d'Ydewalle C, Moonens K, Goethals S, de Winter V, et al. Small heat-shock protein HSPB1 mutants stabilize microtubules in Charcot-Marie-Tooth Neuropathy. J Neurosci 2011; 31: 15320–8.

Antonellis A, Ellsworth RE, Sambuughin N, Puls I, Abel A, Lee-Lin SQ, et al. Glycyl tRNA synthetase mutations in Charcot-Marie-Tooth disease type 2D and distal spinal muscular atrophy type V. Am J Hum Genet 2003; 72: 1293–99.

Benoy V, Vanden Berghe P, Jarpe M, Van Damme P, Robberecht W, Van Den Bosch L. Development of improved HDAC6 inhibitors as pharmacological therapy for axonal Charcot–Marie–Tooth disease. Neurotherapeutics 2017; 14: 417–28.

Butler KV, Kalin J, Brochier C, Vistoli G, Langley B, Kozikowski AP. Rational design and simple chemistry yield a superior, neuroprotective HDAC6 inhibitor, tubastatin A. J Am Chem Soc 2010; 132: 10842–6.

d'Ydewalle C, Krishnan J, Chiheb DM, Van Damme P, Irobi J, Kozikowski AP, et al. HDAC6 inhibitors reverse axonal loss in a mouse model of mutant HSPB1-induced Charcot-Marie-Tooth disease. Nat Med 2011; 17: 968–74.

De Vos KJ, Grierson AJ, Ackerley S, Miller CCJ. Role of axonal transport in neurodegenerative diseases. Annu Rev Neurosci 2008; 31: 151–73.

De Vreese R, Depetter Y, Verhaeghe T, Desmet T, Benoy V, Haeck W, et al. Synthesis and SAR assessment of novel Tubathian analogs in the pursuit of potent and selective HDAC6 inhibitors. Org Biomol Chem 2016; 14: 2537–49.

De Vreese R, Van Steen N, Verhaeghe T, De Smet T, Bougarne N, De Bosscher K, et al. Synthesis of benzothiophene-based hydroxamic acids as potent and selective HDAC6 inhibitors. Chem Commun 2015; 51: 9868–71.

Ermanoska B, Motley WW, Leitão-Gonçalves R, Asselbergh B, Lee LTH, De Rijk P, et al. CMT-associated mutations in glycyl- and tyrosyl-tRNA synthetases exhibit similar pattern of toxicity and share common genetic modifiers in Drosophila. Neurobiol Dis 2014; 68: 180–9.

Gibbs KL, Greensmith L, Schiavo G. Regulation of axonal transport by protein kinases. Trends Biochem Sci 2015; 40: 597–610.

Godena VK, Brookes-Hocking N, Moller A, Shaw G, Oswald M, Sancho RM, et al. Increasing microtubule acetylation rescues axonal transport and locomotor deficits caused by LRRK2 RocCOR domain mutations. Nat Commun 2014; 5: 5245.

Gonzalez M, McLaughlin H, Houlden H, Guo M, Yo-Tsen L, Hadjivassilious M, et al. Exome sequencing identifies a significant variant in methionyl-tRNA synthetase (*MARS*) in a family with late-onset CMT2. J Neurol Neurosurg Psychiatry 2013; 84: 1247–9.

Govindarajan N, Rao P, Burkhardt S, Sananbenesi F, Schlüter OM, Bradke F, et al. Reducing HDAC6 ameliorates cognitive deficits in a mouse model for Alzheimer's disease. EMBO Mol Med 2013; 5: 52–63.

Griffin LB, Sakaguchi R, McGuigan D, Gonzalez MA, Searby C, Züchner S, et al. Impaired function is a common feature of neuropathy-associated glycyl-tRNA synthetase mutations. Hum Mutat 2014; 35: 1363–71.

Guo M, Yang XL, Schimmel P. New functions of aminoacyl-tRNA synthetases beyond translation. Nat Rev Mol Cell Biol 2010; 11: 668–74.

Guo W, Naujock M, Fumagalli L, Vandoorne T, Baatsen P, Boon R, et al. HDAC6 inhibition reverses axonal transport defects in motor neurons derived from FUS-ALS patients. Nat Commun 2017; 8: 861.

He W, Bai G, Zhou H, Wei N, White NM, Lauer J, et al. CMT2D neuropathy is linked to the neomorphic binding activity of glycyl-tRNA synthetase. Nature 2015; 526: 710–14.

Hutchins JR, Toyoda Y, Hegemann B, Poser I, Hériché JK, Sykora MM, et al. Systematic analysis of human protein complexes identifies chromosome segregation proteins. Science 2010; 328: 593–9.

Jordanova A, Irobi J, Thomas FP, Van Dijck P, Meerschaert K, Dewil M, et al. Disrupted function and axonal distribution of mutant tyrosyl-tRNA synthetase in dominant intermediate Charcot-Marie-Tooth neuropathy. Nat Genet 2006; 38: 197–202.

Kalmar B, Innes A, Wanisch K, Koyen Kolaszynska A, Pandraud A, Kelly G, et al. Mitochondrial deficits and abnormal mitochondrial retrograde axonal transport play a role in the pathogenesis of

mutant Hsp27 induced Charcot Marie Tooth Disease. Hum Mol Genet 2017; 26: 3313–26.

Kim JY, Woo SY, Hong Y Bin, Choi H, Kim J, Choi H, et al. HDAC6 inhibitors rescued the defective axonal mitochondrial movement in motor neurons derived from the induced pluripotent stem cells of peripheral neuropathy patients with HSPB1 mutation. Stem Cells Int 2016; 2016: 9475981.

Latour P, Thauvin-Robinet C, Baudelet-Méry C, Soichot P, Cusin V, Faivre L, et al. A major determinant for binding and aminoacylation of tRNAAla in cytoplasmic Alanyl-tRNA synthetase is mutated in dominant axonal Charcot-Marie-Tooth disease. Am J Hum Genet 2010; 86: 77–82.

Leandri M, Ghignotti M, Emionite L, Leandri S, Cilli M. Electrophysiological features of the mouse tail nerves and their changes in chemotherapy induced peripheral neuropathy (CIPN). J Neurosci Methods 2012; 209: 403–9.

Lewis RA, Li J, Fuerst DR, Shy ME, Krajewski K. Motor unit number estimate of distal and proximal muscles in Charcot-Marie-Tooth disease. Muscle Nerve 2003; 28: 161–7.

Martin S, Van Veen S, Holemans T, Demirsoy S, Van Den Haute C, Baekelandt V, et al. Protection against mitochondrial and metal toxicity depends on functional lipid binding sites in ATP13A2. Parkinsons Dis 2016; 2016: 9531917.

McLaughlin HM, Sakaguchi R, Liu C, Igarashi T, Pehlivan D, Chu K, et al. Compound heterozygosity for loss-of-function lysyl-tRNA synthetase mutations in a patient with peripheral neuropathy. Am J Hum Genet 2010; 87: 560–66.

Miskiewicz K, Jose LE, Yeshaw WM, Valadas JS, Swerts J, Munck S, et al. HDAC6 is a bruchpilot deacetylase that facilitates neurotransmitter release. Cell Rep 2014; 8: 94–102.

Motley WW, Seburn KL, Nawaz MH, Miers KE, Cheng J, Antonellis A, et al. Charcot-Marie-Tooth-linked mutant GARS is toxic to peripheral neurons independent of wild-type GARS levels. PLoS Genet 2011; 7: e1002399.

Nangle LA, Zhang W, Xie W, Yang XL, Schimmel P. Charcot-Marie-Tooth disease-associated mutant tRNA synthetases linked to altered dimer interface and neurite distribution defect. Proc Natl Acad Sci USA 2007; 104: 11239–44.

Niehues S, Bussmann J, Steffes G, Erdmann I, Köhrer C, Sun L, et al. Impaired protein translation in Drosophila models for Charcot-Marie-Tooth neuropathy caused by mutant tRNA synthetases. Nat Commun 2015; 6: 7520.

Pareyson D, Saveri P, Sagnelli A, Piscosquito G. Mitochondrial dynamics and inherited peripheral nerve diseases. Neurosci Lett 2015; 596: 66–77.

Prior R, Van Helleputte L, Benoy V, Van Den Bosch L. Defective axonal transport: a common pathological mechanism in inherited and acquired peripheral neuropathies. Neurobiol Dis 2017; 105: 300–20.

Reilly MM. Sorting out the inherited neuropathies. Pract Neurol 2007; 7: 93–105.

Ryan MC, Zeeberg BR, Caplen NJ, Cleland JA, Kahn AB, Liu H, et al. SpliceCenter: a suite of web-based bioinformatic applications for evaluating the impact of alternative splicing on RT-PCR, RNAi, microarray, and peptide-based studies. BMC Bioinformatics 2008; 9: 313.

Seburn KL, Nangle LA, Cox GA, Schimmel P, Burgess RW. An active dominant mutation of glycyl-tRNA synthetase causes neuropathy in a Charcot-Marie-Tooth 2D mouse model. Neuron 2006; 51: 715–26.

Shen S, Benoy V, Bergman JA, Kalin JH, Frojuello M, Vistoli G, et al. Bicyclic-capped histone deacetylase 6 inhibitors with improved activity in a model of axonal Charcot-Marie-Tooth disease. ACS Chem Neurosci 2016; 7: 240–58.

Skre H. Genetic and clinical aspects of Charcot-Marie-Tooth's disease. Clin Genet 1974; 6: 98–118.

Sleigh JN, Dawes JM, West SJ, Wei N, Spaulding EL, Gómez-Martín A, et al. Trk receptor signaling and sensory neuron fate are perturbed in human neuropathy caused by *Gars* mutations. Proc Natl Acad Sci USA 2017; 114: E3324–33.

Sleigh JN, Grice SJ, Burgess RW, Talbot K, Cader MZ. Neuromuscular junction maturation defects precede impaired lower motor neuron connectivity in Charcot-Marie-Tooth type 2D mice. Hum Mol Genet 2014; 23: 2639–50.

Spaulding EL, Sleigh JN, Morelli KH, Pinter MJ, Burgess RW, Seburn KL. Synaptic deficits at neuromuscular junctions in two mouse models of charcot–marie–tooth type 2d. J Neurosci 2016; 36: 3254–67.

Stum M, McLaughlin HM, Kleinbrink EL, Miers KE, Ackerman SL, Seburn KL, et al. An assessment of mechanisms underlying peripheral axonal degeneration caused by aminoacyl-tRNA synthetase mutations. Mol Cell Neurosci 2011; 46: 432–43.

Taes I, Timmers M, Hersmus N, Bento-Abreu A, Van Den Bosch L, Van Damme P, et al. Hdac6 deletion delays disease progression in the $SOD1^{G93A}$ mouse model of ALS. Hum Mol Genet 2013; 22: 1783–90.

Van Helleputte L, Benoy V, Van Den Bosch L. The role of histone deacetylase 6 (HDAC6) in neurodegeneration. Res Rep Biol 2014; 5: 1–13.

Vanden Berghe P, Hennig GW, Smith TK. Characteristics of intermittent mitochondrial transport in guinea pig enteric nerve fibers. Am J Physiol Gastrointest Liver Physiol 2004; 286: G671–82.

Vandesompele J, De Preter K, Pattyn F, Poppe B, Van Roy N, De Paepe A, et al. Accurate normalization of real-time quantitative RT-PCR data by geometric averaging of multiple internal control genes. Genome Biol 2002; 3: RESEARCH0034.

Vester A, Velez-Ruiz G, McLaughlin HM, Nisc Comparative Sequencing Program, Lupski JR, Talbot K, et al. A loss-of-function variant in the human Histidyl-tRNA synthetase (HARS) gene is neurotoxic *in vivo*. Hum Mutat 2013; 34: 191–9.

Wan C, Borgeson B, Phanse S, Tu F, Drew K, Clark G, et al. Panorama of ancient metazoan macromolecular complexes. Nature 2015; 525: 339–44.

Wang Z, Leng Y, Wang J, Liao HM, Bergman J, Leeds P, et al. Tubastatin A, an HDAC6 inhibitor, alleviates stroke-induced brain infarction and functional deficits: potential roles of α-tubulin acetylation and FGF-21 up-regulation. Sci Rep 2016; 6: 19626.

Xie W, Nangle LA, Zhang W, Schimmel P, Yang XL. Long-range structural effects of a Charcot-Marie-Tooth disease-causing mutation in human glycyl-tRNA synthetase. Proc Natl Acad Sci USA 2007; 104: 9976–81.

Yao P, Fox PL. Aminoacyl-tRNA synthetases in medicine and disease. EMBO Mol Med 2013; 5: 332–43.

Ye Q, Ji QQ, Yan W, Yang F, Wang ED. Acetylation of lysine ε-amino groups regulates aminoacyl-tRNA synthetase activity in Escherichia coli. J Biol Chem 2017; 292: 10709–22.

Zhang L, Liu C, Wu J, Tao JJ, Sui XL, Yao ZG, et al. Tubastatin A/ACY-1215 improves cognition in Alzheimer's disease transgenic mice. J Alzheimers Dis 2014; 41: 1193–205.

Zhang X, Yuan Z, Zhang Y, Yong S, Salas-Burgos A, Koomen J, et al. HDAC6 modulates cell motility by altering the acetylation level of cortactin. Mol Cell 2007; 27: 197–213.